

Green Synthesis of Upconverting NaYF₄ and NaGdF₄ Materials and Energy Levels Determination

Luidgi Giordano,^{1a} Matheus F. Nunes,^a Verônica C. Teixeira^{1b} and Lucas C. V. Rodrigues^{1b*,a}

^aDepartamento de Química Fundamental, Instituto de Química, Universidade de São Paulo, 05508-000 São Paulo-SP, Brazil

^bLaboratório Nacional de Luz Síncrotron (LNLS), Centro Nacional de Pesquisa em Energia e Materiais (CNPEM), 13083-970 Campinas-SP, Brazil

An alternative green route using a domestic microwave oven to synthesize NaGdF₄:Yb,Tm and NaYF₄:Yb,Er was successfully developed. Decreasing dopants concentration increased the β -NaREF₄/ α -NaREF₄ ratio in NaGdF₄. The scanning electron microscopy (SEM) images of NaGdF₄ showed particles ranging from 500 nm to 1 μ m with formation of aggregates up to 100 μ m, with two different surface morphologies. The NaGdF₄:Yb,Tm emission spectrum showed white-like emission due to Er³⁺ and Eu³⁺ contamination. The bandgaps of undoped NaGdF₄ and NaYF₄ were measured using synchrotron radiation vacuum-UV (VUV) diffuse reflectance, with values of 10.20 eV for the cubic phase and 10.80 eV for the hexagonal phase for both materials. The determination of the RE^{2+/3+} energy level positions in these fluorides sheds new light on the design of efficient upconversion materials.

Keywords: upconversion, microwave assisted solid-state synthesis, bandgap determination

Introduction

Upconverting materials can convert near infrared radiation into visible light. The upconversion phenomenon is a non-linear photoluminescence process in which two or more photons with low energy are converted into a single photon with higher energy. In general, the process is used to convert near infrared (NIR) into visible or UV radiation.^{1,2} The main characteristics of these materials attracted academic interest due to their wide applications, from solar conversion to bioapplications.³⁻⁵ For example, they can be used as biosensors, in bioimaging and photodynamic therapy given the NIR excitation being inside the biological transparency window.⁶⁻¹⁰ In order to get very efficient materials, it is important to have low-phonon energy, high crystallinity and low defect concentration.^{1,11}

One of the most important upconverting materials, NaYF₄ doped with Yb³⁺ and Er³⁺ was first reported by Menyuk *et al.*¹² in 1972. Hitherto almost 2,000 papers were already published (as observed in the literature search with the terms “NaYF₄” and “upconversion”). These sodium-rare earth fluorides are considered among the most efficient

materials for upconversion as they account for ideal characteristics for upconversion, such as air, water and chemical stability, non-hygroscopicity, and low phonon energy, reducing efficiency loss in upconversion by non-radiative pathways.^{13,14}

In solid-state science the energy of the forbidden band is primary information in the design of new applied compounds. In optical materials, for example, this information can be used to determine which energy levels are accessible, possible suppression mechanisms, potential emission sites and excitation sources, etc.¹⁵ Once in possession of this knowledge, one may have better control in the design of new materials.

Even though these fluorides are heavily studied, having great importance in science today, the determination of experimental bandgap of these materials was reported only once for NaYF₄ in the literature by Krupa *et al.*¹⁶ in 1999, without even much flaunting over it. This parameter is hard to determine since the bandgap of these materials should be in the high energy region (vacuum-UV, VUV) since it is a highly ionic material with fluoride anion, and the experimental setup is further complicated by the necessity of a diffuse reflectance setup coupled to a VUV beamline. In conjunct with spectroscopic data for Ce³⁺ and

*e-mail: lucascvr@iq.usp.br

approximations for other materials' data, it is possible to use this information to determine the energy levels of rare earths in these materials.

Traditionally, upconverting materials are either synthesized as nanoparticles (UCNP) in a thermal decomposition method utilizing 1-octadecene and oleic acid,¹⁷⁻¹⁹ or as microparticles in time-consuming solid-state synthesis,²⁰ but different synthetic methods are also being developed.^{21,22} Solid-state synthesis using microwave dielectric heating have shown great economy in the energy needed to synthesize a large number of ceramics,²³⁻²⁸ aligned with the 6th principle of Green Chemistry: design for energy efficiency. The use of domestic ovens for these syntheses proved to be efficient, reproducible (with parameter optimization), accessible and cost-effective.²⁶

This work aims to show a new energy- and time-saving solid-state synthetic route to make these materials, with a domestic microwave (MW) oven as heating source, and to determine experimentally the bandgap of both NaYF₄ and NaGdF₄ phases and, for the first time, the energy levels of rare earths for the hexagonal lattices.

Experimental

Fluorides synthesis

For the synthesis of NaGdF₄ and NaYF₄, NaF (99% Alfa Aesar, Ward Hill, USA) was used without purification and the RE₃F₃ starting materials were prepared as follows. RE₂O₃ (RE = Y, Gd, Yb, Tm, Er, 99.99%, CSTARM, Shanghai, China) were all separately dissolved with excess of concentrated HNO₃ (LabSynth, São Paulo, Brazil) in hot water, with further adjustment of pH to ca. 5 by evaporation of excess HNO₃ and water addition. The RE³⁺ ions were precipitated as RE₃F₃ by slow addition of stoichiometric amount of NaF solution, then vacuum filtrated. The resultant solid was dried at 100 °C for 6 h and after cooling down, it was pulverized and heated at 400 °C for 4 h in a muffle oven to remove possible hydration water.

In order to get different doping compositions, stoichiometric amounts of RE₃F₃ (RE: Gd, Yb and Tm or Y, Yb and Er) and NaF were mixed in a 1:1 molar proportion totalizing 500 mg of precursors. The MW experimental setup is the same as used by de Carvalho *et al.*²⁴ with the only alteration being the change from 14 to 12 g of activated carbon (1-2 mm, LabSynth, São Paulo, Brazil), in a Electrolux MEF41 (1000 W, São Paulo, Brazil) domestic MW oven. The precursor is put into a small crucible, which is then placed inside a larger crucible, containing activated carbon used as MW susceptor to heat the precursors. The usage of activated carbon also creates a reducing

environment with the *in situ* formation of CO to avoid the formation of oxyfluoride materials. The powers and times used for NaGdF₄ and NaYF₄ are shown on Table S1 (Supplementary Information (SI) section).

Characterization

X-ray powder diffraction (XRD) measurements were performed at 30 kV and 14 mA in a Bruker D2Phaser diffractometer (São Paulo, Brazil) using Cu as anode ($K\alpha = 1.54059 \text{ \AA}$) in a Bragg-Brentano arrangement with 2θ from 10 to 70°. The upconversion spectroscopy measurements were carried with a Horiba Fluorolog 3 using a 980 nm diode laser as the light source (Advanced Optical Spectroscopy Multiuser Laboratory from the Institute of Chemistry from the University of Campinas LMEOA/IQ/UNICAMP, Campinas, Brazil). The electron microscopy work has been performed with a FEI Inspect F50 equipment at the Brazilian Nanotechnology National Laboratory (LNNano, Campinas, Brazil) with 5 keV voltage and Spotsize 2.

In order to get the data on the materials bandgap via diffuse reflectance, a new setup for the VUV beamline (TGM, LNLS, Campinas, Brazil) was developed. The reflectivity signal was recorded at room temperature and pressure of 1×10^{-7} mbar at the Toroidal Grating Monochromator (TGM)²⁹ beamline from the Brazilian Synchrotron Light Laboratory (LNLS). A setup with two similar homemade sodium salicylate-based films (2.5 mol L^{-1} in methanol, deposited via spray method, heated at 80 °C), a microchannel plate (MCP, R3809U-52, from Hamamatsu, Hamamatsu City, Japan), an electrometer (Keithley 6514, Cleveland, USA) and a rotatable stage was mounted on the standard chamber to acquire the data. The excitation energy ranged from 10.0 to 15.7 eV, using the lower energy grating-75 gr mm⁻¹, Pt coated, produced by HORIBA Jobin Yvon, (New Jersey, USA) which ranges from 3 to 16 eV and presents higher performance from 3-13 eV, filtered by gases (0.6 mbar Ne + 0.1 mbar Ar, cut-off: 15.7 eV) to avoid the signal contamination from higher order harmonics. The sample, positioned on the chamber center, was in powder form, glued on an aluminum sample holder with carbon tape. It was irradiated and the reflected photons excited a sodium salicylate film positioned ca. 30° with the beam. The signal was maximized by the adjustment of the sample angular position, which was ca. 15° with the beam. It was integrated by the MCP and read in the current mode. The recorded signal was normalized by the direct beam measured in a second sodium salicylate film positioned at the end of the chamber.

Results and Discussion

The influence of power and time in the MW synthesis is related to the temperature reached by the sample. The higher the power for a fixed time, the higher the temperature. Using different powers in the same synthesis allows a fine tune in the temperature since the first power (normally larger) increases the temperature and the second keeps this temperature with small variations. de Carvalho *et al.*²⁴ using a similar apparatus showed that heating at 300 W during 10 min should achieve a temperature of ca. 450 °C, which is close to the optimal temperature for the NaYF₄ hexagonal phase.³⁰ Since the cubic and hexagonal phases are temperature-dependent, these parameters were modified in order to get the tetrafluorides hexagonal phase with the minimum amount of impurities. For the NaGdF₄:49%Yb,1%Tm materials, the XRD analysis (Figure 1a) indicates that at lower times with 300 W power, there is a large amount of REF₃ impurities. With times longer than 11 min at 300 W there is no presence of this unreacted material, forming a mixture of cubic and hexagonal tetrafluorides.

The peaks appear slightly displaced compared to the pure NaREF₄ phase standards suggesting the formation of

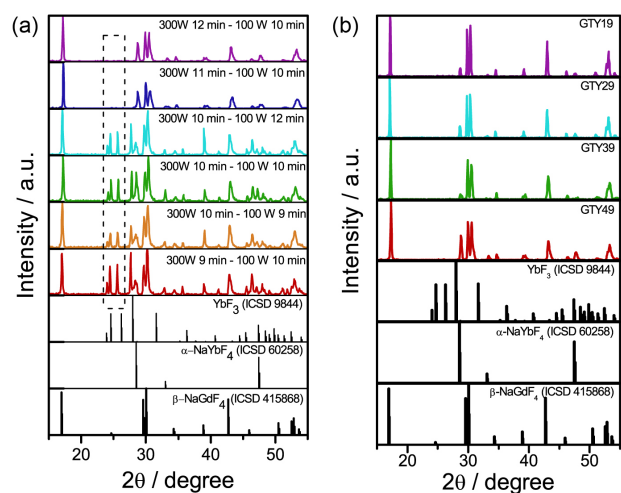


Figure 1. XRD pattern of (a) NaGdF₄:49%Yb,1%Tm prepared with different synthesis conditions and (b) NaGdF₄:X%Yb,1%Tm with different Yb³⁺ doping concentrations. The choice of literature standards^{31–33} relates to the availability of data for the rare-earth fluoride materials in the Inorganic Crystal Structure Database (ICSD). The dashed rectangle shows the disappearance of unreacted REF₃ in higher times at 300 W.

a solid solution for these systems due to the high dopant concentration. The unreacted REF₃ phase disappears with increasing power and time. This is expected from the phase diagram of NaF:REF₃,³⁴ Thoma *et al.*³⁴ showed that, under even higher temperatures, all rare earths from Pr onwards tend to go to the cubic phase or orthorhombic phases when there is a 1:1 equivalence on NaF and REF₃. This behavior is more pronounced for the smaller rare earths like Yb and Y.³⁴ To avoid the presence of REF₃ phase and to have higher reproducibility, the setup of 12 min at 300 W and 10 min at 100 W was chosen to synthesize different compositions of NaGdF₄:Yb,Tm, with the same 1:1 REF₃:NaF stoichiometry (Table 1).

From the XRD data of the materials prepared with different composition (Figure 1b), the percentage of cubic and hexagonal phase was estimated using the following equation according to Ghosh and Patra:³⁵

$$X_c = I_c(111) / [I_h(100) + I_h(110) + I_c(111) + I_h(101) + I_h(201) + I_h(211)] \quad (1)$$

where X_c is the molar fraction of the cubic form, I_c and I_h are the integrated area of the reflections for the cubic and hexagonal phases, respectively.

It is observed that a lower concentration of the NaGdF₄ cubic phase is obtained with decreasing Yb³⁺ doping from 49 to 39%, without remaining REF₃ (Table 1). The hexagonal phase was described as a better phase for upconversion,² so it is preferable to get a higher purity hexagonal phase even if it is necessary to decrease the Yb³⁺ sensitizer concentration.

The MW-assisted synthetic pathway was used for NaYF₄ as well. The XRD patterns (Figure S1, SI section) of the materials prepared with different conditions show that there is no remaining unreacted REF₃, but as observed for NaGdF₄, there is always the contamination from cubic phase. Since Y³⁺ (0.90 Å, coordination number (CN): 6) is smaller than Gd³⁺ (0.94 Å), it is expected that getting a pure hexagonal phase is less probable for NaYF₄. Besides, due to the similarity of the ionic radii of Y³⁺ and Yb³⁺ (0.87 Å), the effect of reducing the concentration of Yb³⁺ dopant is not as pronounced as in the Gd host. Thus, we present the results for only one composition with different

Table 1. Chemical composition of NaGdF₄:Yb,Tm samples and cubic-hexagonal phase percentage

Sample	GdF ₃ / mol%	YbF ₃ / mol%	TmF ₃ / mol%	Cubic phase / %	Hexagonal phase / %
GTY49	50	49	1	14.2	85.8
GTY39	60	39	1	5.5	94.5
GTY29	70	29	1	8.6	91.4
GTY19	80	19	1	5.8	94.2

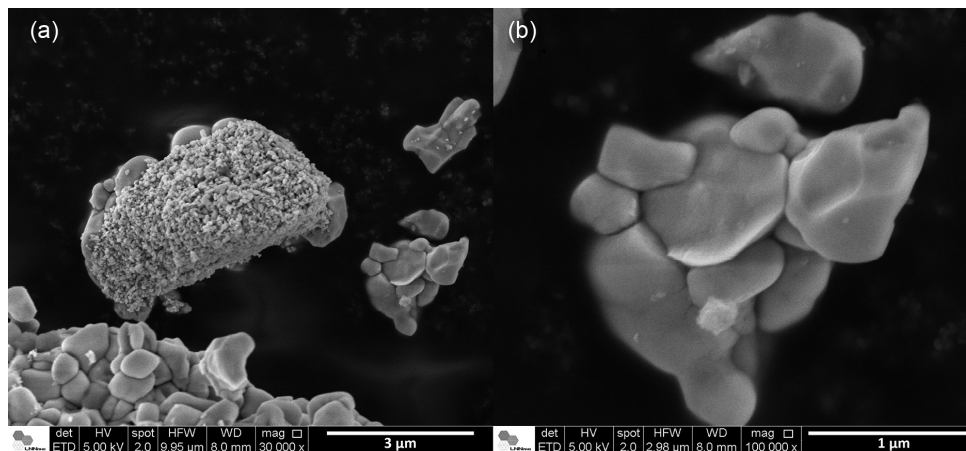


Figure 2. SEM image of GTY39 morphology in different magnifications. (a) 30000 times. (b) 100000 times.

powers and times. One can notice that with a fixed 10 min window at 300 W, the increase in time from 10 to 15 min at 100 W decreases the concentration of the cubic phase. However, when the time at 300 W is increased to 11 min, the concentration of the cubic phase increases. This is in consonance with Laihininen *et al.*³⁰ who showed that the formation of a metastable cubic α -NaYF₄ happens first, followed by a phase transition to the hexagonal β -NaYF₄ with increasing temperature. If temperature continues to increase, there is another phase transition back to α -NaYF₄. The increase in the 300 W time from 10 to 11 min causes a large temperature rise, leading the system to the phase transitions from β - to α -NaYF₄. On the other hand, the increase in the 100 W time leads to a small increase in temperature that favors the formation of the hexagonal phase, which can also be happening due to longer times favoring kinetic parameters. Therefore, this method is more favored for bigger lanthanides as Gd. For Y, the best synthetic method is 10 min at 300 W, followed by 15 min at 100 W.

The micrographs of the GTY39 particles observed by scanning electron microscopy (SEM) (Figure 2) indicate that the materials tend to form large particles with ca. 500 nm-1 μ m size (Figures 2a and 2b). Sintering probably occurred since it is possible to observe large aggregates, due to high temperatures, creating a porous and rough surface. It is also possible to observe two different kinds of surfaces in the particle, probably due to the presence of both hexagonal and cubic phase, with different surfaces.

Spectroscopic measurements

The upconversion emission spectra of all NaGdF₄:X%Yb,1%Tm (Table 1) materials with excitation at 980 nm can be used to determine the optimal Yb³⁺

concentration (Figure 3). The emission spectra exhibit the peaks arising from transitions from Tm³⁺, Er³⁺ and Eu³⁺. Even though no Er or Eu were added to the sample, it is very hard to separate Eu³⁺ from Gd³⁺ and Er³⁺ from Yb³⁺. Yb-Er upconversion is extremely efficient, and Er³⁺ is even considered in some mechanisms of upconversion with other metals.³⁶ The Eu³⁺ upconversion is not very common, but was observed due to two main reasons: (i) since the host is composed of Gd³⁺, a higher concentration of Eu³⁺ impurities is expected²³ and (ii) the mechanism of energy transfer from Tm³⁺ to Eu³⁺ proved to be very efficient in fluorides as pointed out by Lucchini *et al.*³⁷ who showed that the ⁵D₂ and ⁵D₁ Eu³⁺ excited states are efficiently populated via energy transfer from Tm³⁺ ¹G₄ and ¹D₂ excited states.

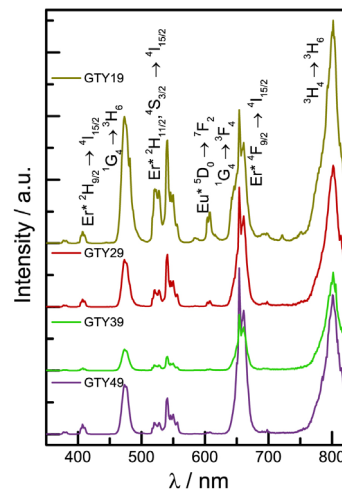


Figure 3. Emission spectra of four different doped-NaGdF₄:x%Yb,1%Tm (x = 19, 29, 39, 49%) prepared by MW-assisted synthesis with 174 mW power (21.8 W cm⁻²) diode laser. Differences in Yb³⁺ concentration change the relative proportion in Tm³⁺ emissions.

Regarding the Tm³⁺ emission, the NIR transition (³H₄ → ³H₆) is the most efficient, mainly because it

is a two photons excitation process, while the more energetic ones (e.g., $^1G_4 \rightarrow ^3H_6$) need three or more photons.^{37,38} One can observe that the relative intensity of Tm³⁺ emission *versus* Er³⁺ impurities increases with decreasing Yb³⁺ concentration. With lower Yb³⁺ concentration, there are less Er³⁺ impurities and therefore there is lower Tm³⁺ emission suppression by energy transfer to Er³⁺. Furthermore, the sample with the lowest amount of Yb³⁺ has the lowest concentration of cubic phase contamination which might enhance Tm³⁺ emission. Some typical upconversion emissions for the NaGdF₄:Yb,Tm, namely, Tm³⁺ $^1D_2 \rightarrow ^3F_4$ emission and Gd³⁺ $^6P_{7/2} \rightarrow ^8S_{7/2}$ are absent, even though they were reported before for this compound synthesized with other methods.³⁸ The absence of those emissions can be related to an energy transfer from these states to other ions, such as the contaminants.

For NaYF₄, the emission spectrum (Figure S2, SI section) has only the expected peaks from literature in two and three-photon mechanisms for the Yb³⁺, Er³⁺ pair.^{39,40} The red dominance can be explained by both the presence of cubic phase and the high concentration of Yb³⁺.⁴⁰

The position of the lanthanide energy levels related to the valence band plays a major role in the efficiency of several luminescence phenomena.⁴¹ However, for upconversion this has been ignored. This happens because the most important process for this phenomenon (energy transfer from Yb³⁺ to activator) depends mainly on the resonance between the excited states, which is independent on the relative positions of these ions in the bandgap. Advances in lanthanide energy levels as dopants in upconversion lattices may lead to further advancements in new upconversion processes, especially those involving 5d levels, different oxidation states or even upconversion-induced persistent luminescence. Here, we construct the first energy levels diagram for the famous NaREF₄ upconverting materials.

Following the same synthetic pathway, undoped NaGdF₄ and NaYF₄ were synthesized, and the diffuse

reflectance was measured in VUV region (Figures 4a and 4b). The poor signal-to-noise ratio is a consequence of the low flux in the synchrotron beamline for this energy region. For both materials, the bandgap is ca. 10.20 (± 0.05) eV for cubic phase and 10.80 (± 0.05) eV for hexagonal phase. The band close to 10.80 bandgap (Figure 4b) is probably the exciton related to the β-NaYF₄, however, due to the low flux in the region, it is not possible to make an accurate attribution. The cubic phase having a smaller bandgap is in accord to the theoretical calculations of Huang *et al.*⁴² The values for the NaYF₄ hexagonal phase are in concordance with the data reported by Krupa *et al.*¹⁶ NaYF₄ and NaGdF₄ having similar bandgaps is expected since they are highly ionic solids with the same anion, same crystalline phase, where both cations (Y³⁺ and Gd³⁺) have very similar electronegativities.

Using both the experimental bandgap and theoretical data from Dorenbos,⁴³ which are based on the centroid shift of Ce³⁺ 4f-5d transition of the materials, we constructed the energy level diagram for β-NaGdF₄ and β-NaYF₄ (Figures 5a and 5b). For both materials, all RE³⁺ ions are stable dopants since all of their ground states are below the Fermi level. On the other hand, differently from several other fluorides materials,⁴⁴ no divalent form of the RE²⁺ dopants (even the most stable ones Eu²⁺ and Yb²⁺) should be expected without the use of strong reducing agents,⁴⁵ due to the position of their ground states above the Fermi level.

These diagrams exhibit the absolute position of the lanthanide ion ground states, and therefore are not essential to explain traditional upconversion mechanisms, since they normally depend on the energy difference between ground and excited states of the lanthanide ions, and not on their position. However, for non-traditional upconversion processes involving divalent lanthanides and 4f-5d states such as CsCaX₃:Tm²⁺ (X: Cl, Br and I),⁴⁶ and upconversion-induced persistent luminescence,⁴⁷ they may help solve mechanisms that are up-to-now unknown.

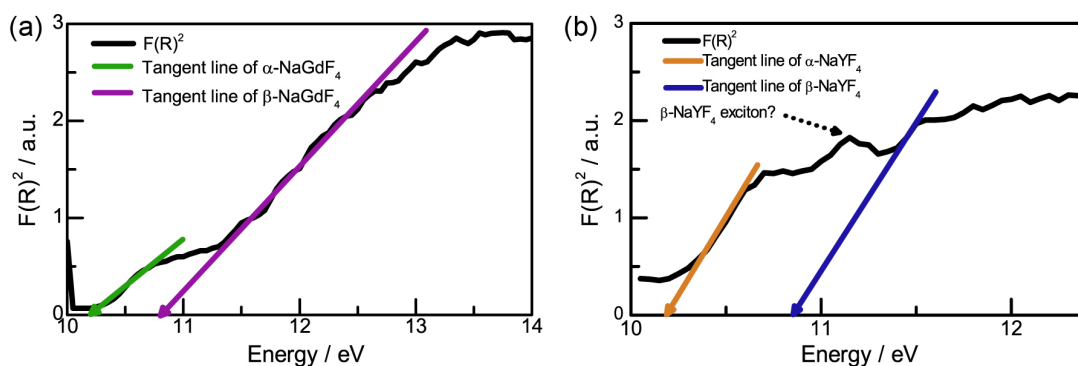


Figure 4. Tauc plot for indirect allowed transitions in undoped NaREF₄ (RE = Gd, Y). The extrapolation of the tangent lines to the abscissa yields the optical bandgap of the material. (a) NaGdF₄. (b) NaYF₄.

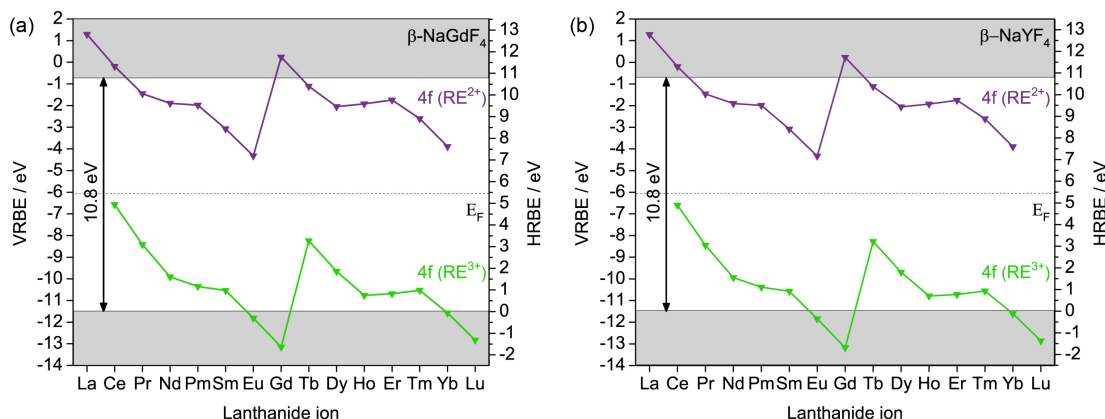


Figure 5. Energy level diagram with the relative position of the ground state of lanthanide dopants for (a) NaGdF₄. (b) NaYF₄.

Conclusions

It is possible to synthesize tetrafluoride upconverting materials such as NaGdF₄:Yb,Tm and NaYF₄:Yb,Er employing green synthesis using a domestic microwave system. The optimized setup uses powers not larger than 300 W and times as long as 25 min. Efficient upconversion emission can be observed from different activators in both hosts. A new synchrotron setup allowed the determination of the experimental bandgap for both cubic and hexagonal phases. These results led to the construction of a host-referred binding energy diagram that showed that all RE³⁺ ions are stable as dopants, but none of the RE²⁺ ions are stable without the use of reducing agents during synthesis. This diagram can offer new light on the study of these very well-known compounds.

Supplementary Information

Supplementary information for the experimental microwave setups for NaGdF₄ and NaYF₄, NaYF₄ XRD diffractogram and upconversion spectrum are available free of charge at <http://jbcs.sbq.org.br> as PDF file.

Acknowledgments

The authors would like to thank FAPESP (2018/05280-5) and CNPq (427312/2016-7, 141252/2017-0 and 101811/2019-5) for financial support, the Electron Microscopy Laboratory (LME) from LNNano (proposal No. 23479) for technical support during electron microscopy work, the TGM beamline and the LNLS team (proposal No. 20190116) for the diffuse reflectance setup and support, both LNNano and LNLS, from the Brazilian Center for Research in Energy and Materials (CNPEM), and Prof Paulo Cesar de Sousa Filho from University of Campinas (UNICAMP) for spectroscopic measurements.

Author Contributions

The manuscript was written through contributions of all authors. All authors have given approval to the final version of the manuscript.

References

1. Auzel, F.; *Chem. Rev.* **2004**, *104*, 139.
2. Baziulyte-Paulaviciene, D.; Karabanovas, V.; Stasys, M.; Jarockyte, G.; Poderys, V.; Sakirzanovas, S.; Rotomskis, R.; *Beilstein J. Nanotechnol.* **2017**, *8*, 1815.
3. de Wild, J.; Meijerink, A.; Rath, J. K.; van Sark, W. G. J. H. M.; Schropp, R. E. I.; *Energy Environ. Sci.* **2011**, *4*, 4835.
4. Chen, G.; Qiu, H.; Prasad, P. N.; Chen, X.; *Chem. Rev.* **2014**, *114*, 5161.
5. Li, Z.; Zhang, Y.; La, H.; Zhu, R.; El-Banna, G.; Wei, Y.; Han, G.; *Nanomaterials* **2015**, *5*, 2148.
6. Sun, Y.; Feng, W.; Yang, P.; Huang, C.; Li, F.; *Chem. Soc. Rev.* **2015**, *44*, 1509.
7. Wang, F.; Liu, X.; *Chem. Soc. Rev.* **2009**, *38*, 976.
8. Ward, M. D.; *Coord. Chem. Rev.* **2007**, *251*, 1663.
9. Kobayashi, H.; Ogawa, M.; Alford, R.; Choyke, P. L.; Urano, Y.; *Chem. Rev.* **2010**, *110*, 2620.
10. Yun, S. H.; Kwok, S. J. J.; *Nat. Biomed. Eng.* **2017**, *1*, 0008.
11. Vendruscolo, V.; Giordano, L.; Constantino, V. R. L.; Rodrigues, L. C. V.; *New J. Chem.* **2020**, *44*, 10165.
12. Menyuk, N.; Dwight, K.; Pierce, J. W.; *Appl. Phys. Lett.* **1972**, *21*, 159.
13. Tiwari, S. P.; Maurya, S. K.; Yadav, R. S.; Kumar, A.; Kumar, V.; Joubert, M.-F.; Swart, H. C.; *J. Vac. Sci. Technol. B* **2018**, *36*, 060801.
14. Naccache, R.; Yu, Q.; Capobianco, J. A.; *Adv. Opt. Mater.* **2015**, *3*, 482.
15. Dorenbos, P.; *J. Lumin.* **2007**, *122-123*, 315.
16. Krupa, J. C.; Queffelec, M.; Kirikova, N. Y.; Makhov, V. N.; *Mater. Sci. Forum* **1999**, *315-317*, 27.

17. Wang, J.; Wang, F.; Xu, J.; Wang, Y.; Liu, Y.; Chen, X.; Chen, H.; Liu, X.; *C. R. Chim.* **2010**, *13*, 731.
18. Wang, F.; Deng, R.; Liu, X.; *Nat. Protoc.* **2014**, *9*, 1634.
19. Palo, E.; Tuomisto, M.; Hyppänen, I.; Swart, H. C.; Hölsä, J.; Soukka, T.; Lastusaari, M.; *J. Lumin.* **2017**, *185*, 125.
20. Liu, H.; Zhang, X.; Wang, N.; Bai, Z.; Gao, X.; Lu, L.; Liu, Q.; Mi, X.; Sun, H.; Wang, X.; *J. Mater. Sci.: Mater. Electron.* **2018**, *29*, 7531.
21. Pang, T.; Peng, W.; Yang, M.; Xie, J.; Lu, W.; *J. Rare Earths* **2018**, *36*, 1136.
22. Pathak, T. K.; Kumar, A.; Erasmus, L. J. B.; Pandey, A.; Coetsee, E.; Swart, H. C.; Kroon, R. E.; *Spectrochim. Acta, Part A* **2019**, *207*, 23.
23. Machado, I. P.; Pedroso, C. C. S.; de Carvalho, J. M.; Teixeira, V. C.; Rodrigues, L. C. V.; Brito, H. F.; *Scr. Mater.* **2019**, *164*, 57.
24. de Carvalho, J. M.; Pedroso, C. C. S.; Machado, I. P.; Hölsä, J.; Rodrigues, L. C. V.; Gluchowski, P.; Lastusaari, M.; Brito, H. F.; *J. Mater. Chem. C* **2018**, *6*, 8897.
25. Pedroso, C. C. S.; Carvalho, J. M.; Rodrigues, L. C. V.; Hölsä, J.; Brito, H. F.; *ACS Appl. Mater. Interfaces* **2016**, *8*, 19593.
26. Levin, E. E.; Grebenkemper, J. H.; Pollock, T. M.; Seshadri, R.; *Chem. Mater.* **2019**, *31*, 7151.
27. Birkel, A.; Denault, K. A.; George, N. C.; Doll, C. E.; He, B.; Mikhailovsky, A. A.; Birkel, C. S.; Hong, B.; Seshadri, R.; *Chem. Mater.* **2012**, *24*, 1198.
28. Perera, S. S.; Munasinghe, H. N.; Yatooma, E. N.; Rabuffetti, F. A.; *Dalton Trans.* **2020**, *49*, 7914.
29. Cavasso Filho, R. L.; Lago, A. F.; Homem, M. G. P.; Pilling, S.; de Brito, A. N.; *J. Electron Spectrosc. Relat. Phenom.* **2007**, *156-158*, 168.
30. Laihininen, T.; Lastusaari, M.; Pihlgren, L.; Rodrigues, L. C. V.; Hölsä, J.; *J. Therm. Anal. Calorim.* **2015**, *121*, 37.
31. Bukvetskii, B. V.; Garashina, L. S.; *Koord. Khim.* **1977**, *3*, 1024.
32. Roy, D. M.; Roy, R.; *J. Electrochem. Soc.* **1964**, *111*, 421.
33. Aebischer, A.; Hostettler, M.; Hauser, J.; Krämer, K.; Weber, T.; Güdel, H. U.; Bürgi, H. B.; *Angew. Chem., Int. Ed.* **2006**, *45*, 2802.
34. Thoma, R. E.; Insley, H.; Hebert, G. M.; *Inorg. Chem.* **1966**, *5*, 1222.
35. Ghosh, P.; Patra, A.; *J. Phys. Chem. C* **2008**, *112*, 3223.
36. Hölsä, J.; Laihininen, T.; Laamanen, T.; Lastusaari, M.; Pihlgren, L.; Rodrigues, L. C. V.; Soukka, T.; *Phys. B: Condens. Matter* **2014**, *439*, 20.
37. Lucchini, G.; Speghini, A.; Canton, P.; Vetrone, F.; Quintanilla, M.; *Nanoscale Adv.* **2019**, *1*, 757.
38. Wang, F.; Deng, R.; Wang, J.; Wang, Q.; Han, Y.; Zhu, H.; Chen, X.; Liu, X.; *Nat. Mater.* **2011**, *10*, 968.
39. Dong, H.; Sun, L. D.; Yan, C. H.; *Nanoscale* **2013**, *5*, 5703.
40. Zhou, J.; Liu, Q.; Feng, W.; Sun, Y.; Li, F.; *Chem. Rev.* **2015**, *115*, 395.
41. Dorenbos, P.; *J. Phys.: Condens. Matter* **2003**, *15*, 8417.
42. Huang, B.; Dong, H.; Wong, K. L.; Sun, L. D.; Yan, C. H.; *J. Phys. Chem. C* **2016**, *120*, 18858.
43. Dorenbos, P.; *J. Lumin.* **2013**, *135*, 93.
44. Dorenbos, P.; *J. Phys.: Condens. Matter* **2003**, *15*, 2645.
45. Su, Y.; Li, P.; Li, G.; *Cryst. Growth Des.* **2008**, *8*, 2678.
46. Grimm, J.; Beurer, E.; Gerner, P.; Güdel, H. U.; *Chem.-Eur. J.* **2007**, *13*, 1152.
47. Li, Z.; Huang, L.; Zhang, Y.; Zhao, Y.; Yang, H.; Han, G.; *Nano Res.* **2017**, *10*, 1840.

Submitted: November 30, 2020

Published online: April 16, 2021

